

Article

# Open-Air Processing of Mechanically Robust Metal Halide Perovskites with Controllable Thicknesses Above 10 µm

Kayshavi Bakshi 1, Muzhi Li 1, Muneeza Ahmad 1, Mason Mahaffey 1 and Nicholas Rolston 1,\*

- Renewable Energy Materials and Devices Lab, School of Electrical, Computer and Energy Engineering (ECEE), Arizona State University, Tempe, AZ, USA
- \* Correspondence: nicholas.rolston@asu.edu

Abstract: We report on the use of open-air blade-coating as a scalable method for producing metal halide perovskite films with >10x fracture energy for durability and mechanical stability through the addition of corn starch polymer additives. This results in a manufacturable and robust perovskite that has tunable thicknesses exceeding 10 µm, among the highest reported values for solution-processed polycrystalline films. We find that an increasing amount of starch causes more uniform carbon distribution within the perovskite thickness as quantified by cross-sectional elemental composition measurements. Further, the incorporation of starch introduces beneficial compressive film stresses. Importantly, the optoelectronic behavior is not compromised, as the photoluminescence spectrum becomes more homogenous with the addition of corn starch up to 20% by weight.

**Keywords:** perovskite solar cells; stability; reliability; blade coating; hyperspectral photoluminescence; fracture; durability; X-ray diffraction; additive; polymer

Citation: Bakshi, K.; Li, M.; Ahmad, M.; Mahaffey, M.; Rolston, N. Open-Air Processing of Mechanically Robust Metal Halide Perovskites with Controllable Thicknesses Above 10 µm. *Processes* **2024**, *volume number*, x.

https://doi.org/10.3390/xxxxx

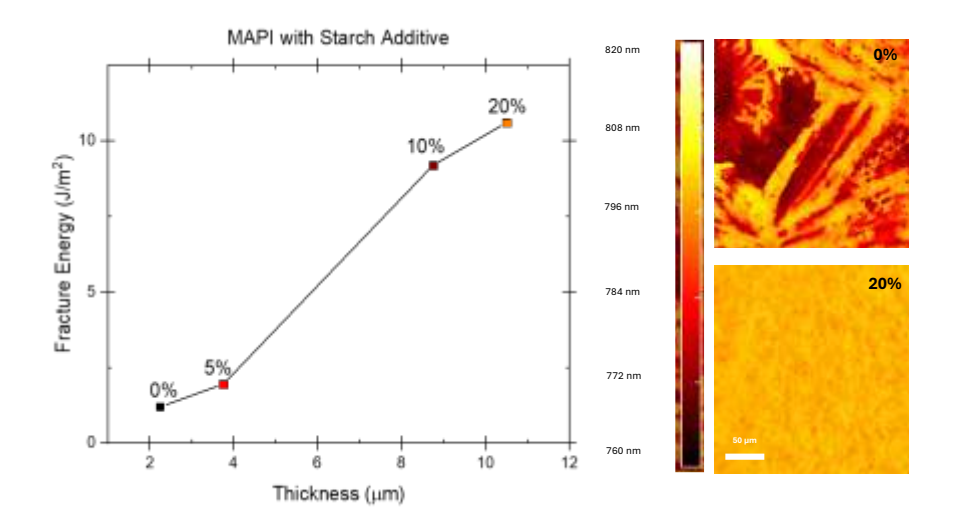
Academic Editor(s): Name

Received: date Revised: date Accepted: date Published: date



Copyright: © 2024 by the authors. Submitted for possible open access publication under the terms and conditions of the Creative Commons Attribution (CC BY) license (https://creativecommons.org/license s/by/4.0/).

## **Graphical Abstract**



# 1. Introduction

Up until recently, the mechanical properties and durability of perovskites were long disregarded. Many recent studies have focused on strain engineering

perovskites to reduce internal degradation and improve optoelectronic properties. The fracture energy (G<sub>c</sub>) is now being studied more commonly to better understand the mechanical properties of Perovskite Solar Cells (PSCs) and perovskite films [1-10]. The fracture energy,  $G_c$ , is the strain energy per unit area that is required to generate a crack through a material and quantifies the robustness or durability of materials. Ge is dependent on two processes: plastic deformation and atomic bond breakage. Within materials that are plastically deformable, the energy to break their atomic bonds is generally much lower than the energy needed for plastic deformation. However, due to their fragile and brittle nature, the Go of perovskites is largely due to atomic bond breakage. In fact, perovskites have such weak ionic bonding that their G<sub>c</sub> is often comparable to table salt. Furthermore, the thin film layers that make up PSCs-including the perovskite itself-are susceptible to high stresses and strain-induced delamination [11]. This is due to the weak, low-adhesion bonds between the layers, especially when small molecules are involved such as fullerenes. The stresses and weak bonds within the films can eventually lead to fracture and layer delamination within the material. Fracturing and delamination of PSCs can further damage the device and accelerate environmental degradation by allowing moisture and loss of the organic cations in the perovskite structure. Accelerated degradation caused by fracture and delamination can result in the loss of ohmic contact, leading to compromises in power conversion efficiency (PCE) and device failure.

PSCs have quickly developed over the last 10-15 years. They have improved from a 3.8% record PCE to >25% record PCE in just over a decade [12–15]. Yet, PSCs are currently not competitive with their silicon alternatives when it comes to their long-term operational stability. Past studies have found that the fracture energy of PSCs are consistently <  $1.5 \text{ J/m}^2$ , while c-Si cells are ~  $10-200 \text{ J/m}^2$  [11]. The robust covalent bonds between silicon atoms enable higher toughness, leading to > 25-year operational lifetimes above 80% of their initial performance [16]. Investigating the fracture energy of perovskite is therefore significant to increase their operational longevity.

Along with operational longevity, scaling PSC manufacturing is another important factor for the future of these devices. Currently, different film fabrication techniques are used between lab and industry, with no dominant method emerging for long-term scaled perovskite manufacturing [17]. Spin coating is a film fabrication technique that has been widely used to create uniformly dense and stable perovskite films but is restricted to the physical substrate size [18]. Other fabrication methods such as blade-coating and slot die coating are particularly promising due to their ability to be done in the open air on flexible substrates, affordability, and industrial scalability [19,20]. However, this comes with the challenge of controlling film crystallization since the use of an antisolvent is challenging. There are many studies which have discussed solvent engineering and quenching approaches to enable PSCs with blade-coating and the similarly designed slot-die coating technique [21–23].

Additive engineering is a method that can be used to improve both the robustness and scalability of perovskite. The addition of starch additives to perovskite also aids in the fabrication of a film with controlled crystallization in a single anti-solvent-free and quench-free step using blade-coating. The incorporation of polymer additives, such as corn starch or gellan gum, enables the tuning of various properties of perovskite and shows promising effects in reducing film degradation and aiding in stability [24]. Specifically, it has been shown that a small amount of ionic liquid additive to the perovskite precursor aided in passivating non-radiative

recombination due to defects at the grain boundaries [24]. It was shown that the incorporation of starch into perovskite imparts hygroscopic abilities that protects the perovskite from moisture and the ambient environment [25,26]. Other work observed a retention of 50% of initial PCE after aging tests of spin-coated MAPI films with starch additive, credited due to the protection effect from ambient contamination from the hygroscopic starch [25]. The same study found that the addition of starch enabled the formation of a high-quality film with optimized band energy alignment resulting in a respectable PCE of 18.8% demonstrating the ability of non-conductive additives that do not compromise device performance [25]. Regarding robustness and stability, the plasticity of corn starch improves the resistance of the perovskite to bending stresses. Previous reports suggest that corn starch aids in trapping the cation and reducing structural decomposition, resulting in a more stable film under thermal cycling and moderate humidity when compared to unmodified perovskite [25,26]. Additive engineering with starch and similar non-conducting polymers has also shown promising results in improving operational stability. One study tested gellan gum and starch additives in MAPI films in aging conditions at 85% humidity for 100 hours. These samples with additives took longer to visibly degrade, displaying the improved stability both starch and gellan gum impart on MAPI films [8]. Another experiment involving thermal cycling of MAPI with additives between -40 and 85°C for 200 cycles supports the additives' ability to stabilize the perovskite films due to inducing compressive intrinsic stresses within the film [8]. Compressive film stresses are one of the desirable film properties when fabricating perovskite devices as they impart self-healing properties and stability to the perovskite film. A critical aspect of film fabrication is tuning the thickness of the perovskite for optimal properties such as film morphology, power conversion efficiency, and stability. Previously, the thickness of spin coated perovskite films has been controlled by molarity and concentration adjustments of the precursors or through spin speed [27-29]. These methods allow easy control of film thicknesses that range from a few hundred nanometers to 1 µm. The incorporation of additives to the perovskite structure offers a new avenue to engineer the viscosity of the precursor solution and fabricate thicker films (1-15 µm thick). The addition of corn starch and polymer additives to perovskite precursor results in more viscous solutions, allowing for better control over deposition and coverage using blade-coating methodology. The creation of thicker films is particularly useful for high-energy detection applications such as X-ray and alpha/beta radiation detection, as recent work has demonstrated tuning the viscosity of the ink to enable ultra-thick (~100 µm) films using CsPbBr<sub>3</sub> [30]. This is desirable because the thicker the active layer in an x-ray detector, the direct absorption of high energy species will be improved [31]. Furthermore, perovskites are well-suited for higher absorption applications due to the composition of large atomic number elements such as lead [Pb] and Iodine [I] [32,33]. In addition, the large radiation resistance, processing versatility, and their defect tolerant nature makes perovskites a great potential candidate for high energy detection [31,32,34–37].

In this work, we study the effect of a corn starch additive on the mechanical properties, stability, and microstructure of methylammonium lead iodide, CH<sub>3</sub>NH<sub>3</sub>PbI<sub>3</sub> (MAPI). We investigate the elemental composition and optical property changes that occur with the addition of corn starch with the use of X-Ray Diffraction and photoluminescence testing. The objective of this research was to improve mechanical durability and develop a scalable, open air fabrication method of MAPI perovskite films through the incorporation of corn starch polymers. Altogether, this study utilizes processing techniques and solution-additive engineering to simultaneously improve the robustness of perovskite and ensure future scalability.

#### 2. Materials and Methods

The MAPI ink is made by combining MAI and PbI<sub>2</sub> in a ratio of 159 mg MAI: 461 mg PbI<sub>2</sub> to 1 mL Dimethyl Sulfoxide (DMSO). This solution is then mixed in a FisherBrand Vortex Mixer until homogenous. Once these perovskite precursors are dissolved, it can be used to make the 5wt%, 10wt%, and 20wt% starch weight concentration inks. Specifically, to make a 5% weight concentration, 31mg of starch was added to 1 mL of 1.0M MAPI ink. The corn-starch was acquired from Sigma Aldrich Inc. After adding the starch to the inks, it is then placed on a magnetic hot plate with a stir bar to mix until the starch is integrated into the ink. To make the fracture samples, this ink is deposited (20-30 µl) through blade-coating at speed 4 \* 25 mm/s on a preheated glass substrate (40 °C) and annealed at 100 °C for 30 minutes (Fig. 1a). The glass substrates are at least 3 cm long to promote multiple fractures throughout testing. The glass substrate shall either have a layer of Nickel Oxide (NiO, spin-coated) or be ITO glass (Indium Tin Oxide) to create roughness. Once the perovskite ink is deposited on the glass substrate, two protective layers are then deposited. These protective layers are to prevent epoxy deformation from contributing to the perovskite fracture energy. Tested samples had layers where both layers were polymethyl methacrylate (PMMA) or with 1-layer PMMA and 1-layer of evaporated silver (Ag) (Fig. 1b). The NiO and PMMA layers are spin coated to evenly distribute the compound across the film. To finish creating a Double Cantilever Beam (DCB) fracture testing sample, a thin layer of epoxy is layered onto an identical-sized glass substrate and bonded to the PSC film. The epoxy is then left to cure overnight at room temperature in an N2 Box. The final fracture testing sample is a sandwichlike-structure where the PSC film layers are between two glass substrates.

Using double cantilever beam testing (DCB), the critical load that is necessary for fracture propagation is found alongside the G<sub>c</sub> value. The sandwiched structure samples are tested by the DCB. A necessary part of this fracture testing is creating a pre-crack in the sample to assist crack formation at the perovskite layer. A pre-crack is made by carefully inserting the tip of a razor in between the sandwiched sample and creating a well defined crack between the two glass substrates (**Fig. 1c**).

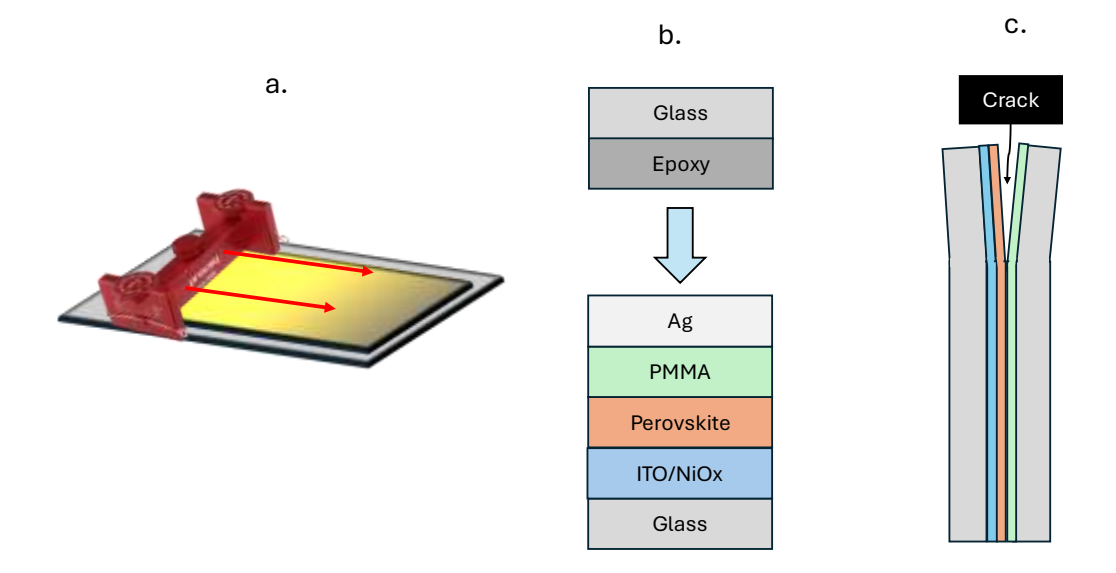


**Figure 1.** Schematics of methods used for sample fabrication and DCB testing. A. blade-coating technique used to deposit perovskite ink with starch. B. Sample fabrication for DCB testing C. DCB crack path through fabricated sample.

Next, the sandwiched sample is loaded in the DCB system with a constant displacement rate until the load suddenly decreases. This sudden decrease represents the critical load that starts the crack propagation throughout the sample. After the sudden drop in load occurs, the sample is then unloaded briefly to obtain a linear region for calculating the crack length. Then, the sample is re-loaded until the next sudden drop in load. The process is then repeated to propagate the crack throughout the sample in cycles. In cycling the sample through loading and unloading cycles, there are additional critical loads correlating with the propagating crack. The Gc can then be calculated for each of these critical loads and averaged to maximize the data per sample using this equation:

$$G_c = \frac{12P_c^2 a^2}{b^2 E h^3} \left( 1 + .64 \frac{h}{a} \right)^2 \tag{1}$$

 $P_c$  is the critical load that deviates from the linear elastic region of the material in the load displacement plot, a is the crack length that is calculated using the compliance method, b and h are the width and height of the sample, and E is the elastic modulus of the glass substrate. The crack length, a, can be calculated using the following equation:

$$a = \left(\frac{d\Delta}{dP} * \frac{BE'^{h^3}}{8}\right)^{\frac{1}{3}} - .64h^2 \tag{2}$$

Where  $\Delta$  is displacement and P represents the applied load. The above equations are used to find the fracture energy as a function of the critical loads it takes to propagate a crack through a material or device stack. In simple terms, fracture energy is

calculated from the energy needed from contributions of breaking bonds and deformation of material, which is in this case a MAPI film.

XRD-sin²  $\psi$  method was used to measure the residual perovskite film stress. This method conducts XRD scans of the sample at various fixed tilt angles ( $\psi$ ) and emit diffraction angles (2 $\theta$ ) [38,39]. After calibrating XRD tool and aligning the sample, an initial 2 $\theta$  scan was taken across a wide range (5-55°). From there, a high angle-high intensity peak is selected to perform the psi-measurements. Scans of the sample are then performed at that peak at a wide range of values of  $\sin^2\!\psi$  ( $\sin^2\!\psi$ =0, 0.05, 0.1, 0.15, 0.2, .25, .3). For the MAPI used in these experiments, a 2 $\theta$  peak at 20 was used to perform  $\sin^2\!\psi$  measurements. 2 $\theta$  is then used define  $d_{\phi\psi}$  (d-spacing of the crystal lattice) that is used in a linear regression of eq.4 to calculate stress. The relationship between 2 $\theta$  and  $d_{\phi\psi}$  is defined by Bragg's law:

$$d_{\phi\psi} = \frac{\lambda_0}{2\sin(2\theta)} \tag{3}$$

Where  $\lambda_0$  is the characteristic wavelength of the incident X-rays used in the XRD analysis. For this analysis, a  $\lambda_0$  of .154 nm was used. Once d-spacing is found with Bragg's relationship with  $2\theta$ , the  $\sin^2\!\psi$  equation below can be used to plot linear regression of d-spacing vs [(1+v)\* $\sin^2\!\psi$ -2v]/E:

$$d_{\phi\psi} = \left[ \left( \frac{1 + v_f}{E_f} \right) \sin^2 \psi - \left( \frac{2v_f}{E_f} \right) \right] \sigma_f d_0 + d_0 \tag{4}$$

E<sub>f</sub> is the Young Modulus of the Film,  $v_f$  is the Poisson ratio of the film,  $\sigma_f$  is the stress within the film,  $d_0$  is the lattice spacing at the stress free or unstrained condition, and  $d_{\varphi\psi}$  is the lattice spacing of the measured plane. For MAPI, the Poisson ratio and Young's modulus used was 0.33 and 15 GPa, respectively. Measuring the peak shifts of the perovskite at different detector tilt angles allows an understanding of how the lattice deforms with the addition of starch. From this equation, residual film stress can be calculated by dividing the slope ( $\sigma_f$  d<sub>0</sub>) by the y-intercept (d<sub>0</sub>).

The Delaminator Adhesion Test Systems (DTS, Menlo Park, CA) is used in DCB configuration to conduct fracture tests. Horiba GD-Profiler 2 Glow Discharge Optical Emission Spectrometer was used to obtain composition profiles of the perovskite films. Using a Tencor P-16 Profilometer and scoring our varying samples, thickness of these blade coated samples was found. A Rigaku Smart Lab X-ray diffractometer was used for X-ray diffraction  $\sin^2 \psi$  analysis. Photon Etc Hyperspectral Imager was used to gather hyperspectral photoluminescence images.

Hyperspectral photoluminescence (PL) measurements were taken using a Photon Etc. IMA hyperspectral microscope [40]. By using a Volume-Bragg grating to select for specific wavelengths, this microscope captures calibrated PL spectra at each pixel of an imaging camera. A 660-nm laser was used to illuminate the sample under a 20x objective. The photon flux at the sample was calibrated to be approximately 1-Sun equivalent by using a Thorlabs PM100D laser power meter (along with knowledge of the illumination area and the assumption that the laser power was perfectly absorbed by the samples). Each image displays an area of approximately 385  $\mu m \times 385 \ \mu m$ .

# 3. Results & Discussion

Perovskite samples containing 0%, 5%, 10%, and 20% weight concentrations of corn starch added directly to the precursor ink were tested. These values were selected based on previous work that demonstrated PSCs that retained high device PCE [41]. From Fig. 2, the control (0wt%) blade-coated MAPI film exhibited a relatively low G<sub>c</sub> of 1.2 ± 0.4 J/m<sup>2</sup> that is comparable with other reports of perovskite fracture energy[42,43]. MAPI with 5wt% starch concentration showed low fracture energy as well, with a value of 1.95 ± 1.3 J/m<sup>2</sup>. 10wt% and 20wt% starch concentration samples displayed significantly higher fracture energies with 9.19 ± 2.4 J/m<sup>2</sup> and 10.6 ± 4.6 J/m<sup>2</sup> values, respectively. There appears to be a threshold starch concentration above which the films are mechanically robust (~10 J/m²) at 10wt% concentration. The 10wt% and 20wt% starch perovskites exceed the manufacturability threshold of 5 J/m<sup>2</sup>, a rule-of-thumb value that enables mechanical robustness of perovskite material against cracking and thin film stresses during manufacturing and operation [44]. We speculate that this could be due to a critical amount of starch enabling increased deformability, modified microstructure, and 'scaffolding' to the perovskite structure [25]. 10 and 20wt% of starch result in a significant 10x improvement to the fracture energy of MAPI, breaching the 5 J/m<sup>2</sup> manufacturability threshold and demonstrating starch as an effective path to long term film durability.

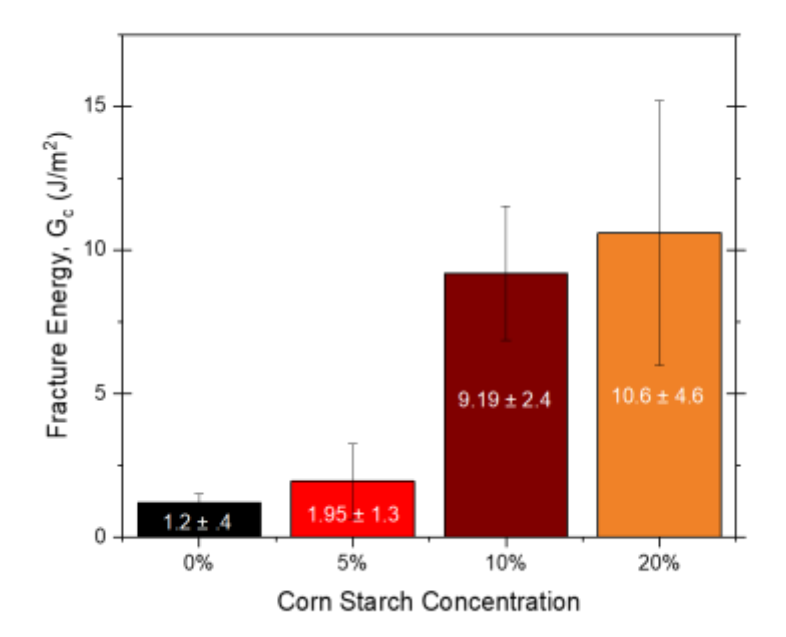
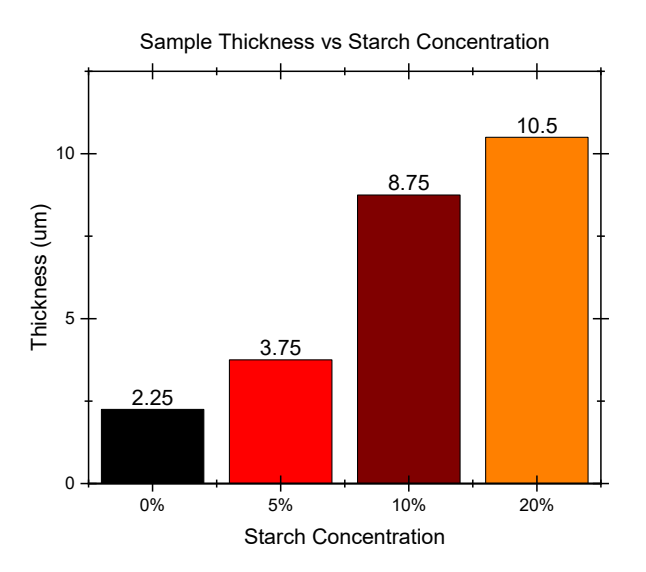


Figure 2. Fracture energy (Gc) of MAPI with 0, 5, 10, and 20wt% concentrations of starch.

The addition of starch made thicker films potentially suitable for other energy detection applications as measured by profilometry after processing (**Fig. S1**). Unmodified blade-coated MAPI had a thin film thickness of ~2.25  $\mu$ m. The increasing addition of starch also increased the thickness. 5wt% starch sample had a thickness of 3.75  $\mu$ m, 10wt% had a thickness of 8.75  $\mu$ m, and 20wt% had a thickness of 10.5  $\mu$ m (**Fig. 3**). The 10 and 20wt% samples thus resulted in both a more durable and substantially thicker film. The increase in film thickness is not necessarily the only reason behind the improvement in mechanical robustness. A previous study has shown that increased fracture energy can occur with thickness changes that are much lower when

starch-MAPI films were spin coated. A spin-coated MAPI films with starch content of 10wt% and 20wt% were previously found to have a thickness of 450 nm and 1.5  $\mu$ m respectively [25]. While the blade-coated thickness of MAPI films with 10wt% and 20wt% starch had thicknesses of 8.75  $\mu$ m and 10.5  $\mu$ m.

The thickness of these blade-coated films is critical to their application, as the films with starch are by far too thick to ideally be used in solar applications [45–47]. A thicker perovskite film can result in the charge carriers recombining before extraction from the device and conversion into a current due to a carrier diffusion length shorter than a micron (nonradiative recombination) [48]. However, thicker perovskite films do have potential in applications for high energy detection due to a thicker active layer with higher absorption length [32-35]. A previous study found that blade-coated MAPI with a thickness of 16.5 µm served as a functioning selfpowered X-ray detector under an irradiation dose rate of 0.2372 mGy<sub>air</sub>s<sup>-1</sup> [49] Other research, found that for optimal X-ray photoconductivity MAPI films should have a thickness is  $\sim 30 \,\mu m$  when used for a conventional CuK<sub> $\alpha$ </sub> X-ray tube source (8 keV) [50]. In general film thicknesses must equal to or be higher than the X-ray absorption length must be selected. These thicker MAPI films may also be suitable for alpha particle detection, as alpha particles are heavy and have a much shorter penetration depth compared to X-rays. The technique displayed here is highly versatile as it offers the ability to control thicknesses of the films over 10 um that can ideally be used in low energy x-ray detection applications.



**Figure 3.** Thickness of MAPI samples with starch additive in 0, 5, 10, and 20wt% concentrations.

To better understand the effect that starch has on the composition of the film cross-section along with its distribution throughout the film, Glow Discharge Optical Emission spectroscopy (GDOES) was used [51,52]. GDOES obtained the elemental composition of samples with 5-20wt% starch. GDOES profiled through the thickness of the sample, sputtering through the perovskite film with cornstarch (C<sub>6</sub>H<sub>10</sub>O<sub>5</sub>), to the glass substrate (as indicated by sodium, Na) (**Fig. 4**). The control and 5wt% starch concentration samples reached the substrate as evidenced by the increase in Na more quickly than the 10wt% and 20wt%. This increase in Na more quickly is due to the higher thicknesses that the 10 wt% and 20wt% films have (**Fig. 3**). Furthermore, the

control and 5wt% starch concentration samples had decreasing carbon composition while the 10wt% and 20wt% starch had stable or increasing carbon compositions. Carbon becomes more evenly dispersed and uniform throughout the sample as starch content increases. This is suggestive that the starch is incorporated throughout each sample. Interestingly, the oxygen signal is not as uniformly distributed, and it shows a larger concentration near the buried interface with the glass for the 10 wt% and 20 wt% starch concentrations. Since oxygen is also a component of the starch, this does suggest that there could be a slightly higher presence near the bottom of the film. The increased amount of carbon—indicating the presence of starch—is hypothesized to reinforce the perovskite microstructure and enable higher  $G_c$  values.

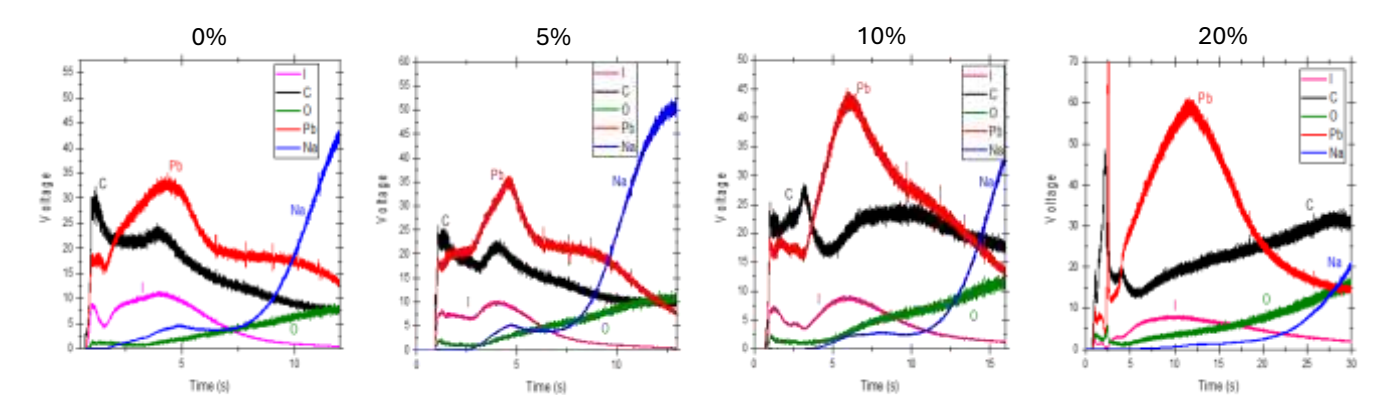


**Figure 4.** Glow Discharge Optical Electron Spectroscopy (GDOES) depth profiles of ambient blade-coated MAPI samples with 0, 5, 10, and 20wt% concentrations of starch.

X-ray diffraction was used to study the effect of starch on the residual perovskite film stress after processing using the sin<sup>2</sup> $\psi$  method (**Fig. S2a-S2d**). Without any starch, the 0wt% showed a tensile film stress of 27 MPa. Residual tensile stress is expected and widely reported after processing, as perovskites have a much higher thermal expansion coefficient than glass [38]. Compressive stresses were observed with 5wt% and higher concentrations of starch additive (Fig. 5). 5wt% starch resulted in the largest compressive stress at -65 MPa. Additionally, this behavior agrees with previous work that found that the addition of gellan gum and starch polymers induced compressive stresses and translates to blade coated perovskites [8]. Interestingly, the compressive stress induced by the additive was found to be lower in magnitude with higher starch additive concentration. 10wt% and 20wt% starch additions exhibited slightly less compressive stresses at -46 and -41 MPa respectively. This effect could be due to the substantial increase in film thickness which generates internal stress that can offset some of the compressive stress from processing. Compressive stresses within the perovskite are beneficial to the film due to the increased stability and potential healing properties they impart on structural defects [53].

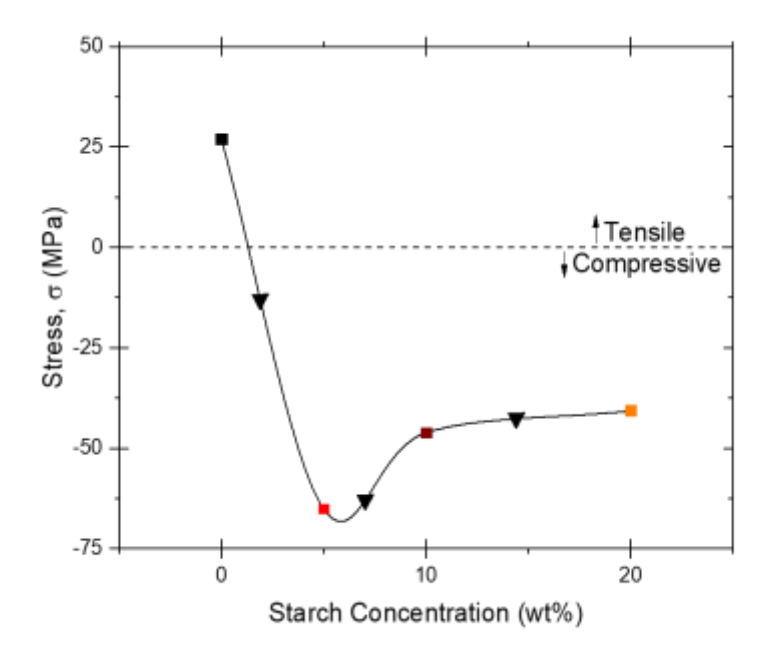


**Figure 5.** Thin film residual stress measurements from X-Ray Diffraction  $\sin^2 \psi$  analysis of the 0, 5, 10, and 20wt% MAPI-starch samples that were ambient blade-coated on glass.

Optoelectronic properties were studied using hyperspectral photoluminescence to map the effect of starch on the emission of MAPI films. From Figure 6, the photoluminescence intensity of the samples at 760nm increased with starch concentration from ~1013 photons/(cm2\*s\*eV\*sr) without starch (Fig. 6a) to ~1014 photons/(cm<sup>2</sup>\*s\*eV\*sr with 5wt% (**Fig. 6b**) to ~10<sup>15</sup> photons/(cm<sup>2</sup>\*s\*eV\*sr) with 10wt% and ~1016 photons/(cm2\*s\*eV\*sr) with 20wt% (Fig. 6d). From 0wt% to 20wt% starch, there was about 3 orders of magnitude increase in photoluminescence intensity. This observed higher photoluminescence intensity is expected and likely due in part to increased thickness due to the starch. The effect starch has on improving photoluminescence intensity indicates higher built-in voltage, an effect which correlates to the Voc (open circuit voltage) in a device. Photoluminescence intensity offers insight into the photoexcited charge-carrier density which corresponds to the magnitude of the Voc in a device [54]. Here, the photoluminescence is seen to improve with the addition of starch, suggesting that starch may be able to improve the Voc of a photovoltaic device. This conclusion agrees with previous work that observed a PCE of 18.8% with 10wt% of starch additive [25].

The hyperspectral images also offer insight into the morphology of the films with starch. The inclusion of starch aids in the uniformity of peak wavelength at which the film is most luminescent (**Fig. S3-S6**). Specifically, the 0wt% starch has a variation in emission peak that varies by 42 nm as seen in **Fig. 6e**. Starch addition at 5wt% had a range of 17 nm (**Fig. 6f**) while 10wt% had a wavelength emission range of 25 nm (**Fig. 6g**). This variation in emission reduced to 5 nm in the 20wt% starch film as seen across image **Fig. 6h**. Altogether, the addition of the starch additive resulted in more compact and uniform morphology as well as more uniform wavelength peak emission—suggestive of a more homogeneous film and correlating directly with

morphology improvements from the starch addition—than unmodified MAPI. The addition of starch shows better film morphology, suggesting that there are less defects in the film, which is also seen to correlate to optimal optoelectronic performance and structural improvement relating to mechanical robustness.

The experiments conducted in this study have shown that starch additive effectively aids in film stability while creating a mechanically robust film. The starch's beneficial behavior is comparable to that of biopolymer additive gellan gum. Previous work has found that 0.56wt% of gellan gum resulted in a similar fracture energy of 10.9 J/m<sup>2</sup> [55]. Interestingly, when compared to gellan gum, blade-coated MAPI films with starch have significantly higher thicknesses. Earlier work has shown that blade coated films with 0.56wt% gellan gum had thickness of 200 nm while the work in this study found that 5wt% of starch resulted in a film thickness of 3.75 µm [8]. Gellan gum was also seen to similarly improve photoluminescence intensity of MAPI films. Other work has shown that biopolymer additives can also reduce phase segregation in mixed halide perovskites [56]. In comparison to other additives, starch has been shown to effectively thicken and improve the morphology of MAPI films, making this method particularly advantageous for applications that require thicker active layers. This study offers an advantage in using scalable, single-step, open-air processing to improve fracture energy of perovskite films while simultaneously adjusting morphology and thickness over a wide range for X-ray, alpha, and beta particle detection applications.

Based on the ability to create high quality films greater than 10 µm thick, further investigations should be conducted on the practical high energy detection applications of perovskite with starch additives. In particular, it will be necessary to investigate the potential effects of X-rays on the starch within the MAPI films. It could be worthwhile to investigate high detection applications with other additives as well. For instance, there is the opportunity to utilize additives such as gellan gum that result in a thicker film with less weight concentration added due to its higher viscosity [8]. Comparative high energy detection studies of perovskites with various additives could offer further insight into the development of a tunable, durable, and scalable perovskite film. Importantly, a key question remains of the resistance that biopolymer additives will offer against high-energy sources, as organic materials typically are more readily decomposed. There is an opportunity to use fully inorganic perovskite compositions (Cs in place of MA as the A-site) and to perform a sintering or solvent removal step of the additive, but the effect this will have on the mechanical robustness and morphology remains unknown [57].

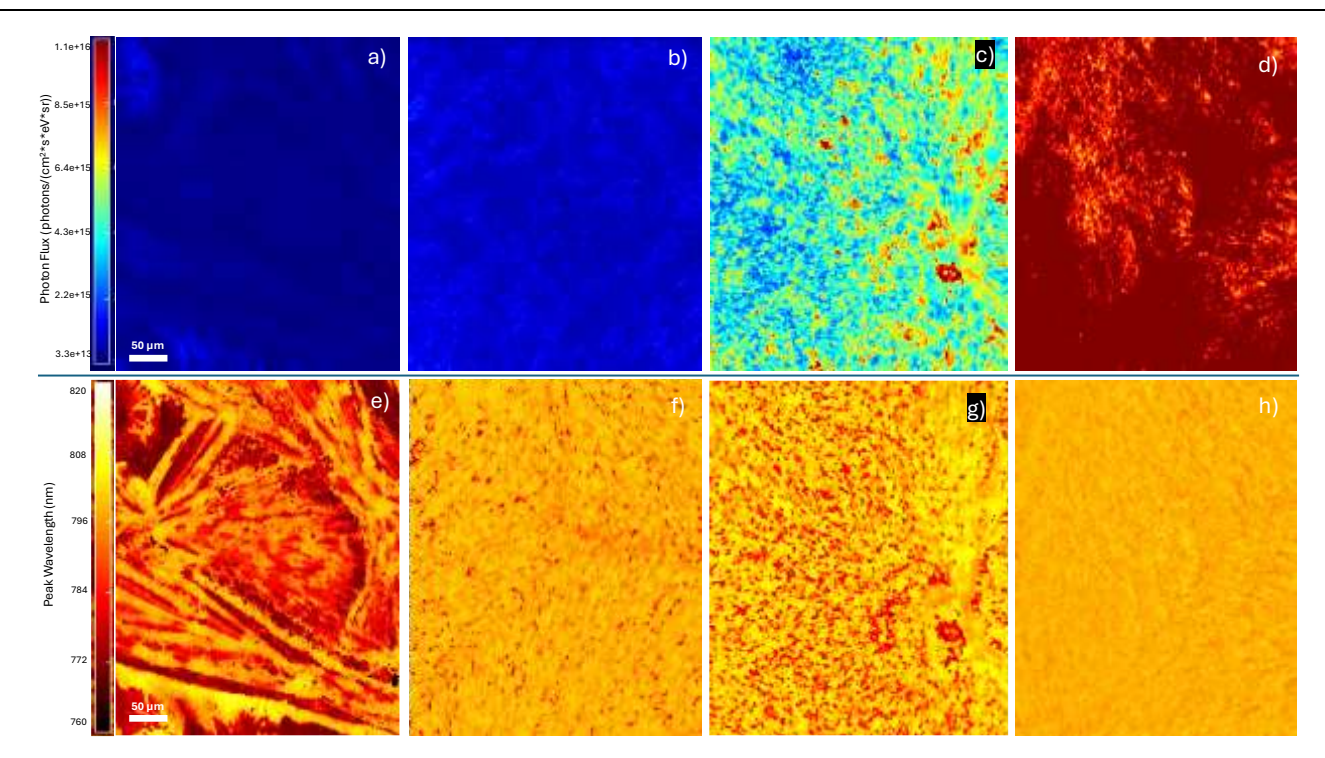


**Figure 6.** Hyperspectral photoluminescence images of the MAPI films that were ambient blade-coated on glass with starch additives. Where the tope row a-d) are photoluminescence intensity profiles and the bottom row e-h) are the wavelength profiles. The first column (a & e) are of 0% starch, b & f are of 5% starch, c & g are of 10% starch, and d & h are of 20% starch. The field of view in all images is the same. In the top row of intensity profiles, higher starch concentrations c) and d) reached higher photoluminescence intensities. Higher starch concentrations were seen to cause more uniform wavelength profiles in g) and h) specifically.

## 4. Conclusion

This work elaborates on the mechanism behind and implications of improved fracture energy from starch additives in metal halide perovskite films. The key result is that starch concentration of 10wt% and above results in a ~10x increase in fracture energy, and changes in structural and elemental properties can be used to explain this improvement. The starch acts as reinforcement to the perovskite based on its uniform distribution throughout the film. It also acts as thickener of the film, where 10wt% starch resulted in a ~4x thicker film than plain MAPI. Starch was further observed to induce desirable compressive film stresses within the perovskite, indicating higher mechanical stability especially due to the simultaneous increase in fracture energy. The use of starch was also seen to enhance the uniformity and photon flux from hyperspectral photoluminescence measurements of the perovskite. Overall, the processes used in this study offer a strategy to create tunable, open-air, and scalable strategy to make durable perovskite films.

**Acknowledgments:** This material is based upon work supported by the National Science Foundation under Grant No. 2339233. The authors also acknowledge the use of facilities within the Eyring Materials Center at Arizona State University supported in part by NNCI-ECCS-1542160. The authors acknowledge resources and support from the Advanced Electronics and Photonics Core Facility at Arizona State University.

**Conflicts of Interest:** The authors have no conflicts of interest to report.

# Data Availability Statement: Data will be made available upon reasonable request.

#### References

- 1. Dai, Z.; Padture, N.P. Challenges and Opportunities for the Mechanical Reliability of Metal Halide Perovskites and Photovoltaics. *Nat Energy* **2023**, *8*, 1319–1327, doi:10.1038/s41560-023-01378-6.
- 2. Dai, Z.; Doyle, M.C.; Liu, X.; Hu, M.; Wang, Q.; Athanasiou, C.E.; Liu, Y.; Sheldon, B.W.; Gao, H.; Liu, S. (Frank); et al. The Mechanical Behavior of Metal-Halide Perovskites: Elasticity, Plasticity, Fracture, and Creep. *Scr Mater* **2023**, 223, doi:10.1016/j.scriptamat.2022.115064.
- 3. Dai, Z.; Yadavalli, S.K.; Hu, M.; Chen, M.; Zhou, Y.; Padture, N.P. Effect of Grain Size on the Fracture Behavior of Organic-Inorganic Halide Perovskite Thin Films for Solar Cells. *Scr Mater* **2020**, *185*, 47–50, doi:10.1016/j.scriptamat.2020.03.044.
- 4. Li, M.; Johnson, S.; Gil-Escrig, L.; Sohmer, M.; Figueroa Morales, C.A.; Kim, H.; Sidhik, S.; Mohite, A.; Gong, X.; Etgar, L.; et al. Strategies to Improve the Mechanical Robustness of Metal Halide Perovskite Solar Cells. *Energy Advances* **2023**, *3*, 273–280, doi:10.1039/d3ya00377a.
- 5. Seong, S.; Liu, Y.; Gong, X. Mechanical Study of Perovskite Solar Cells: Opportunities and Challenges for Wearable Power Source. *Opt Mater Express* **2022**, *12*, 772, doi:10.1364/ome.450214.
- 6. Seong, S.; Liu, Y.; Gong, X. Mechanical Study of Perovskite Solar Cells: Opportunities and Challenges for Wearable Power Source [Invited]: Supplement., doi:10.6084/m9.figshare.18665504.
- 7. McAndrews, G.R.; Guo, B.; Morales, D.A.; Amassian, A.; McGehee, M.D. How the Dynamics of Attachment to the Substrate Influence Stress in Metal Halide Perovskites. *APL Energy* **2023**, *1*, doi:10.1063/5.0177697.
- 8. Ahmad, M.; Cartledge, C.; McAndrews, G.; Giuri, A.; McGehee, M.D.; Rizzo, A.; Rolston, N. Tuning Film Stresses for Open-Air Processing of Stable Metal Halide Perovskites. *ACS Appl Mater Interfaces* **2023**, *15*, 51117–51125, doi:10.1021/acsami.3c11151.
- 9. Yadavalli, S.K.; Chen, M.; Hu, M.; Dai, Z.; Zhou, Y.; Padture, N.P. Electron-Beam-Induced Cracking in Organic-Inorganic Halide Perovskite Thin Films. *Scr Mater* **2020**, *187*, 88–92, doi:10.1016/j.scriptamat.2020.05.062.
- 10. Ramirez, C.; Yadavalli, S.K.; Garces, H.F.; Zhou, Y.; Padture, N.P. Thermo-Mechanical Behavior of Organic-Inorganic Halide Perovskites for Solar Cells. *Scr Mater* **2018**, *150*, 36–41, doi:10.1016/j.scriptamat.2018.02.022.
- 11. Rolston, N.; Scheideler, W.J.; Flick, A.C.; Chen, J.P.; Elmaraghi, H.; Sleugh, A.; Zhao, O.; Woodhouse, M.; Dauskardt, R.H. Rapid Open-Air Fabrication of Perovskite Solar Modules. *Joule* **2020**, *4*, doi:10.1016/j.joule.2020.11.001.
- 12. Kojima, A.; Teshima, K.; Shirai, Y.; Miyasaka, T. Organometal Halide Perovskites as Visible-Light Sensitizers for Photovoltaic Cells. *J Am Chem Soc* **2009**, *131*, doi:10.1021/ja809598r.
- 13. Yoo, J.J.; Seo, G.; Chua, M.R.; Park, T.G.; Lu, Y.; Rotermund, F.; Kim, Y.K.; Moon, C.S.; Jeon, N.J.; Correa-Baena, J.P.; et al. Efficient Perovskite Solar Cells via Improved Carrier Management. *Nature* **2021**, *590*, doi:10.1038/s41586-021-03285-w.
- 14. Min, H.; Lee, D.Y.; Kim, J.; Kim, G.; Lee, K.S.; Kim, J.; Paik, M.J.; Kim, Y.K.; Kim, K.S.; Kim, M.G.; et al. Perovskite Solar Cells with Atomically Coherent Interlayers on SnO2 Electrodes. *Nature* **2021**, *598*, doi:10.1038/s41586-021-03964-8.
- 15. Lin, R.; Xu, J.; Wei, M.; Wang, Y.; Qin, Z.; Liu, Z.; Wu, J.; Xiao, K.; Chen, B.; Park, S.M.; et al. All-Perovskite Tandem Solar Cells with Improved Grain Surface Passivation. *Nature* **2022**, *603*, doi:10.1038/s41586-021-04372-8.
- 16. Peters, I.M.; Hauch, J.; Brabec, C.; Sinha, P. The Value of Stability in Photovoltaics. *Joule* **2021**, *5*, 3137–3153, doi:10.1016/j.joule.2021.10.019.
- 17. Yan, J.; Savenije, T.J.; Mazzarella, L.; Isabella, O. Progress and Challenges on Scaling up of Perovskite Solar Cell Technology. *Sustain Energy Fuels* **2022**, *6*, 243–266, doi:10.1039/d1se01045j.
- 18. Deokate, R. Spin Coating/Doctor-Blading/Self-Assembly of Metal Oxide Nanostructures. In *Solution Methods* for Metal Oxide Nanostructures; 2023.

- 19. Srivastava, A.; Satrughna, J.A.K.; Tiwari, M.K.; Kanwade, A.; Yadav, S.C.; Bala, K.; Shirage, P.M. Lead Metal Halide Perovskite Solar Cells: Fabrication, Advancement Strategies, Alternatives, and Future Perspectives. *Mater Today Commun* 2023, 35.
- 20. Jiao, J.; Yang, C.; Wang, Z.; Yan, C.; Fang, C. Solvent Engineering for the Formation of High-Quality Perovskite Films: A Review. *Results in Engineering* 2023, *18*.
- 21. Geistert, K.; Ternes, S.; Ritzer, D.B.; Paetzold, U.W. Controlling Thin Film Morphology Formation during Gas Quenching of Slot-Die Coated Perovskite Solar Modules. *ACS Appl Mater Interfaces* **2023**, doi:10.1021/acsami.3c11923.
- 22. Fievez, M.; Singh Rana, P.J.; Koh, T.M.; Manceau, M.; Lew, J.H.; Jamaludin, N.F.; Ghosh, B.; Bruno, A.; Cros, S.; Berson, S.; et al. Slot-Die Coated Methylammonium-Free Perovskite Solar Cells with 18% Efficiency. *Solar Energy Materials and Solar Cells* **2021**, 230, doi:10.1016/j.solmat.2021.111189.
- 23. Vesce, L.; Stefanelli, M.; Rossi, F.; Castriotta, L.A.; Basosi, R.; Parisi, M.L.; Sinicropi, A.; Di Carlo, A. Perovskite Solar Cell Technology Scaling-up: Eco-Efficient and Industrially Compatible Sub-Module Manufacturing by Fully Ambient Air Slot-Die/Blade Meniscus Coating. *Progress in Photovoltaics: Research and Applications* **2024**, 32, 115–129, doi:10.1002/pip.3741.
- 24. Shen, D.; Luo, C.; Zheng, R.; Li, Q.; Chen, Y. Improvement of Photoluminescence Intensity and Film Morphology of Perovskite by Ionic Liquids Additive. In Proceedings of the E3S Web of Conferences; EDP Sciences, May 12 2021; Vol. 257.
- 25. Giuri, A.; Rolston, N.; Colella, S.; Listorti, A.; Esposito Corcione, C.; Elmaraghi, H.; Lauciello, S.; Dauskardt, R.H.; Rizzo, A. Robust, High-Performing Maize-Perovskite-Based Solar Cells with Improved Stability. *ACS Appl Energy Mater* **2021**, *4*, doi:10.1021/acsaem.1c02058.
- 26. Hamukwaya, S.L.; Hao, H.; Zhao, Z.; Dong, J.; Zhong, T.; Xing, J.; Hao, L.; Mashingaidze, M.M. A Review of Recent Developments in Preparation Methods for Large-Area Perovskite Solar Cells. *Coatings* 2022, 12.
- 27. Sun, W.; Choy, K.L.; Wang, M. The Role of Thickness Control and Interface Modification in Assembling Efficient Planar Perovskite Solar Cells. *Molecules* **2019**, *24*, doi:10.3390/molecules24193466.
- 28. Park, J.Y.; Song, R.; Liang, J.; Jin, L.; Wang, K.; Li, S.; Shi, E.; Gao, Y.; Zeller, M.; Teat, S.J.; et al. Thickness Control of Organic Semiconductor-Incorporated Perovskites. *Nat Chem* **2023**, *15*, 1745–1753, doi:10.1038/s41557-023-01311-0.
- 29. Liu, D.; Li, Y.; Shi, B.; Yao, X.; Fan, L.; Zhao, S.; Liang, J.; Ding, Y.; Wei, C.; Zhang, D.; et al. Tailoring Morphology and Thickness of Perovskite Layer for Flexible Perovskite Solar Cells on Plastics: The Role of CH3NH3I Concentration. *Solar Energy* **2017**, *147*, 222–227, doi:10.1016/j.solener.2017.03.035.
- 30. Liu, Y.; Gao, C.; Li, D.; Zhang, X.; Zhu, J.; Wu, M.; Liu, W.; Shi, T.; He, X.; Wang, J.; et al. Dynamic X-Ray Imaging with Screen-Printed Perovskite CMOS Array. *Nat Commun* **2024**, *15*, doi:10.1038/s41467-024-45871-2.
- 31. Kakavelakis, G.; Gedda, M.; Panagiotopoulos, A.; Kymakis, E.; Anthopoulos, T.D.; Petridis, K. Metal Halide Perovskites for High-Energy Radiation Detection. *Advanced Science* 2020, 7.
- 32. Huang, K.W.; Li, M.H.; Chen, Y.T.; Wen, Z.X.; Lin, C.F.; Chen, P. Fast Fabrication of Mm-Thick Perovskite Films by Using a One-Step Doctor-Blade Coating Method for Direct X-Ray Detectors. *J Mater Chem C Mater* **2023**, *12*, 1533–1542, doi:10.1039/d3tc02736h.
- 33. Atkinson, N.J.; Evans, J.; Simmonds, D.J.& Material Change for X-Ray Detectors; 2014; Vol. 42;.
- 34. Li, G.; Zhao, C.; Liu, Y.; Ren, J.; Zhang, Z.; Di, H.; Jiang, W.; Mei, J.; Zhao, Y. High-Performance Perovskite Betavoltaics Employing High-Crystallinity MAPbBr3Films. *ACS Omega* **2021**, *6*, 20015–20025, doi:10.1021/acsomega.1c03053.
- 35. Kim, Y.C.; Kim, K.H.; Son, D.Y.; Jeong, D.N.; Seo, J.Y.; Choi, Y.S.; Han, I.T.; Lee, S.Y.; Park, N.G. Printable Organometallic Perovskite Enables Large-Area, Low-Dose X-Ray Imaging. *Nature* **2017**, *550*, 87–91, doi:10.1038/nature24032.
- 36. Romano, V.; Agresti, A.; Verduci, R.; D'Angelo, G. Advances in Perovskites for Photovoltaic Applications in Space. *ACS Energy Lett* 2022, *7*, 2490–2514.

- 37. Lang, F.; Nickel, N.H.; Bundesmann, J.; Seidel, S.; Denker, A.; Albrecht, S.; Brus, V. V.; Rappich, J.; Rech, B.; Landi, G.; et al. Radiation Hardness and Self-Healing of Perovskite Solar Cells. *Advanced Materials* **2016**, *28*, 8726–8731, doi:10.1002/adma.201603326.
- 38. Dailey, M.; Li, Y.; Printz, A.D. Residual Film Stresses in Perovskite Solar Cells: Origins, Effects, and Mitigation Strategies. *ACS Omega* 2021, *6*, 30214–30223.
- 39. Luo, Q.; Jones, A.H. High-Precision Determination of Residual Stress of Polycrystalline Coatings Using Optimised XRD-Sin2ψ Technique. *Surf Coat Technol* **2010**, 205, 1403–1408, doi:10.1016/j.surfcoat.2010.07.108.
- 40. Photon, E. Leverage the Power of Hyperspectral Microscopy.
- 41. Giuri, A.; Masi, S.; Listorti, A.; Gigli, G.; Colella, S.; Esposito Corcione, C.; Rizzo, A. Polymeric Rheology Modifier Allows Single-Step Coating of Perovskite Ink for Highly Efficient and Stable Solar Cells. *Nano Energy* **2018**, *54*, 400–408, doi:10.1016/j.nanoen.2018.10.039.
- 42. Dai, Z.; Yadavalli, S.K.; Hu, M.; Chen, M.; Zhou, Y.; Padture, N.P. Effect of Grain Size on the Fracture Behavior of Organic-Inorganic Halide Perovskite Thin Films for Solar Cells. *Scr Mater* **2020**, *185*, 47–50, doi:10.1016/j.scriptamat.2020.03.044.
- 43. Rolston, N.; Printz, A.D.; Tracy, J.M.; Weerasinghe, H.C.; Vak, D.; Haur, L.J.; Priyadarshi, A.; Mathews, N.; Slotcavage, D.J.; McGehee, M.D.; et al. Effect of Cation Composition on the Mechanical Stability of Perovskite Solar Cells. *Adv Energy Mater* **2018**, *8*, 1702116, doi:10.1002/aenm.201702116.
- 44. Watson, B.L.; Rolston, N.; Printz, A.D.; Dauskardt, R.H. Scaffold-Reinforced Perovskite Compound Solar Cells. *Energy Environ Sci* **2017**, *10*, 2500–2508, doi:10.1039/C7EE02185B.
- 45. Ouslimane, T.; Et-taya, L.; Elmaimouni, L.; Benami, A. Impact of Absorber Layer Thickness, Defect Density, and Operating Temperature on the Performance of MAPbI3 Solar Cells Based on ZnO Electron Transporting Material. *Heliyon* **2021**, *7*, doi:10.1016/j.heliyon.2021.e06379.
- 46. Son, C.; Son, H.; Jeong, B.-S. Enhanced Conversion Efficiency in MAPbI3 Perovskite Solar Cells through Parameters Optimization via SCAPS-1D Simulation. *Applied Sciences* **2024**, *14*, 2390, doi:10.3390/app14062390.
- 47. Rai, M.; Wong, L.H.; Etgar, L. Effect of Perovskite Thickness on Electroluminescence and Solar Cell Conversion Efficiency. *Journal of Physical Chemistry Letters* **2020**, *11*, 8189–8194, doi:10.1021/acs.jpclett.0c02363.
- 48. Shi, P.; Xu, J.; Yavuz, I.; Huang, T.; Tan, S.; Zhao, K.; Zhang, X.; Tian, Y.; Wang, S.; Fan, W.; et al. Strain Regulates the Photovoltaic Performance of Thick-Film Perovskites. *Nat Commun* **2024**, *15*, doi:10.1038/s41467-024-47019-8.
- 49. Tan, J.; Gao, X.; Huang, X.; Wangyang, P.; Sun, H.; Yang, D.; Zeng, T. Self-Powered X-Ray Detector Based on Lead Halide Perovskites under Electric Field Poling Effect. *Journal of Materials Science: Materials in Electronics* **2023**, 34, doi:10.1007/s10854-023-10627-z.
- 50. Yakunin, S.; Sytnyk, M.; Kriegner, D.; Shrestha, S.; Richter, M.; Matt, G.J.; Azimi, H.; Brabec, C.J.; Stangl, J.; Kovalenko, M. V.; et al. Detection of X-Ray Photons by Solution-Processed Lead Halide Perovskites. *Nat Photonics* **2015**, *9*, 444–449, doi:10.1038/nphoton.2015.82.
- 51. Dally, P.; Messou, D.; Robillard, M.; Cacovich, S.; Yaiche, A.; Rousset, J.; Etcheberry, A.; Bouttemy, M. Probing the Chemistry of Perovskite Systems by XPS and GD-OES Depth-Profiling: Potentials and Limitations. In Proceedings of the Conference Record of the IEEE Photovoltaic Specialists Conference; Institute of Electrical and Electronics Engineers Inc., June 20 2021; pp. 931–934.
- 52. Zheng, D.; Volovitch, P.; Pauporté, T. What Can Glow Discharge Optical Emission Spectroscopy (GD-OES) Technique Tell Us about Perovskite Solar Cells? *Small Methods* 2022, 6.
- 53. Rolston, N.; Bush, K.A.; Printz, A.D.; Gold-Parker, A.; Ding, Y.; Toney, M.F.; McGehee, M.D.; Dauskardt, R.H. Engineering Stress in Perovskite Solar Cells to Improve Stability. *Adv Energy Mater* **2018**, *8*, 1802139, doi:10.1002/aenm.201802139.
- 54. Goetz, K.P.; Taylor, A.D.; Paulus, F.; Vaynzof, Y. Shining Light on the Photoluminescence Properties of Metal Halide Perovskites. *Adv Funct Mater* 2020, 30.

- 55. Cartledge, C.; Penukula, S.; Giuri, A.; Bakshi, K.; Ahmad, M.; Mahaffey, M.; Li, M.; Zhang, R.; Rizzo, A.; Rolston, N. Scalable and Quench-Free Processing of Metal Halide Perovskites in Ambient Conditions. *Energies (Basel)* **2024**, *17*, doi:10.3390/en17061455.
- 56. Bisconti, F.; Leoncini, M.; Bravetti, G.; Giuri, A.; Polimeno, L.; Carallo, S.; Colella, S.; Gatto, L.; Grandi, F.; Cinquanta, E.; et al. Blocking Wide Bandgap Mixed Halide Perovskites' Decomposition through Polymer Inclusion. *J Mater Chem C Mater* **2023**, *11*, 12213–12221, doi:10.1039/d3tc01833d.
- 57. Zhao, X.; Liu, T.; Burlingame, Q.C.; Liu, T.; Holleyiii, R.; Cheng, G.; Yao, N.; Gao, F.; Loo, Y.-L. *Accelerated Aging of All-Inorganic, Interface-Stabilized Perovskite Solar Cells*;

**Disclaimer/Publisher's Note:** The statements, opinions and data contained in all publications are solely those of the individual author(s) and contributor(s) and not of MDPI and/or the editor(s). MDPI and/or the editor(s) disclaim responsibility for any injury to people or property resulting from any ideas, methods, instructions or products referred to in the content.